Accounting for Precipitation Asymmetry in a Multiplicative Random Cascades Disaggregation Model

Kaltrina Maloku[1], Benoit Hingray[1], and Guillaume Evin[1]

[1]Univ. Grenoble Alpes, CNRS, INRAE, IRD, Grenoble INP, IGE, 38000 Grenoble, France

Correspondence: Kaltrina Maloku (kaltrina.maloku@univ-grenoble-alpes.fr)

Abstract.

Analytical Multiplicative Random Cascades (MRCs) are widely used for the temporal disaggregation of coarse-resolution precipitation time series. This class of models applies simple scaling laws to represent the dependence of the cascade generator on the temporal scale and the precipitation intensity. Although determinant, the dependence on the external precipitation pattern is usually disregarded. Our work presents a unified MRC modelling framework that allows the cascade generator to depend in a continuous way on temporal scale, precipitation intensity and a so-called precipitation asymmetry index.

Different MRC configurations are compared for 81 locations in Switzerland with contrasted climates. The added value of the dependence of the MRC on the temporal scale appears to be unclear, unlike what was suggested in previous works. Introducing the precipitation asymmetry dependence in the model leads to a drastic improvement of model performance for all statistics related to precipitation temporal persistence (wet/dry transition probabilities, lag-n autocorrelation coefficients, lengths of dry/wet spells). Accounting for precipitation asymmetry seems to solve this important limitation of previous MRCs.

The model configuration that only accounts for the dependence on precipitation intensity and asymmetry is highly parsimonious, with only five parameters, and provides adequate performances for all locations, seasons and temporal resolutions. The spatial coherency of the parameter estimates indicates a real potential for regionalisation and for further application to any location in Switzerland.

1 Introduction

Multi-decadal time series of sub-daily precipitation, hourly or even higher temporal resolution, are necessary for many applications, e.g. assessment of soil erosion (Römkens et al., 2002; Jebari et al., 2012) or of flash floods due to intense precipitation (Rafieeinasab et al., 2015; Liang et al., 2016), hydrological simulation of small catchments, such as those in mountainous
20 regions (Sikorska and Seibert, 2018) or urban areas (Ochoa-Rodriguez et al., 2015; Cristiano et al., 2017). However, fine-scale precipitation data are scarce and usually cover limited periods of time, rarely predating the 80's (Segond et al., 2006; Jennings et al., 2010). In contrast, daily precipitation observations are widely spread worldwide and cover much longer periods, even going back to the middle of the 19th century in some cases. To take benefit from their much richer information, high-resolution precipitation data are often derived from coarse-resolution observations (especially daily) via some appropriate disaggregation
25 process. For a given sequence of daily precipitation amounts, for instance, some disaggregation can be used to generate hourly precipitation scenarios, distributing the precipitation amount observed each day to its different hourly subdivisions. Disaggregation has been widely used to produce high-resolution time series scenarios from observed time series of daily precipitation, e.g. Molnar and Burlando (2005), or from low-resolution synthetic ones obtained in a first step with a so-called stochastic weather generator (e.g. Koutsoyiannis and Onof, 2001; Kang and Ramírez, 2010; Paschalis et al., 2014). Disaggregation mod-
30 els have also been used to generate high-resolution spatial precipitation (multi-site or spatial fields, see e.g. Mezghani and Hingray, 2009; Evin et al., 2018; Viviroli et al., 2022).

Many disaggregation models have been presented in the past. A widely used method is the non-parametric method of fragments (MOF), where the disaggregation scheme for any target day is obtained from the high-resolution temporal (and spatial, if relevant) structure of a given analog day selected in the archive of observations (e.g. Mezghani and Hingray, 2009;
35 Breinl and Di Baldassarre, 2019; Park and Chung, 2020; Acharya et al., 2022). By construction, MOF methods preserve the sub-daily patterns of precipitation and the intermittency properties within each day. An alternative disaggregation method is provided by multiplicative random cascades (MRCs), inspired by the statistical theory of turbulent fields (Schertzer and Lovejoy, 1987; Tessier et al., 1993). Because of the simplicity of both parameter estimation and simulation processes, MRCs have been widely used in the past for many applications in hydrology, for the point temporal disaggregation of precipitation
40 time series (e.g. Menabde and Sivapalan, 2000; Pui et al., 2012; Pohle et al., 2018), or for the spatial-temporal disaggregation of precipitation fields (e.g. Seed et al., 1999; Rupp et al., 2012; Schleiss, 2020).

MRC models are usually implemented with a so-called branching number equal to 2. In such a case, the amount of precipitation at any time step is partitioned into two parts, attributed respectively to the first and second subdivision of this time step. The partition is repeated throughout the cascade levels until the final temporal resolution is achieved (Olsson, 1998; Molnar
45 and Burlando, 2005; Rupp et al., 2009). In the so-called micro-canonical MRC models, the partition of precipitation is conservative. The precipitation amounts R_1 and R_2 attributed respectively to the first and second subdivisions of the considered time step (with precipitation amount R_0), are expressed as $R_1 = W_1 \cdot R_0$ and $R_2 = W_2 \cdot R_0$, where $W_1 + W_2 = 1$. For a given time step, the disaggregation can be determined by the so-called breakdown coefficient assigned to the first subdivision: $W := W_1$ which can take the values 0 with probability p_{01} (no precipitation is attributed to the first subdivision), 1 with probability p_{10}

50 (R_0 is fully attributed to the first subdivision) or any value between 0 and 1. When $W \in (0,1)$, $W^+ = W$ follows a statistical distribution with probability density function f_{W^+}.

The probabilities p_{01}, p_{10} and the distribution f_{W^+} define Γ, the statistical distribution of W, called the cascade generator. For a given location, they have been found to depend on different factors. They first depend on the temporal scale and on the precipitation intensity of the precipitation amount R_0 to disaggregate (e.g. Molnar and Burlando, 2005; Rupp et al., 2009).

55 For instance, p_{01} and p_{10} tend to significantly decrease with precipitation intensity and to be larger for higher time resolution; they also often exhibit some seasonality (Molnar and Burlando, 2008). The cascade generator Γ also depends on the so-called external pattern of precipitation, i.e. on the temporal sequence of precipitation amounts R_{t-1}, R_t, R_{t+1} around the precipitation amount R_t to disaggregate (Ormsbee, 1989; Olsson, 1998; Güntner et al., 2001). For instance, p_{01} tends to be higher and p_{10} smaller in the case of a so-called "ascending" precipitation pattern (when $R_{t-1} < R_t < R_{t+1}$) and, conversely, p_{01} tends to be

60 smaller and p_{10} higher with descending patterns ($R_{t-1} > R_t > R_{t+1}$).

Different models have been proposed for the cascade generator Γ, i.e. for the estimation of p_{01}, p_{10}, and f_{W^+} as a function of selected factors of variability. They are either empirical or analytical. Empirical models are usually obtained from the empirical cumulative distribution function (ECDF) of W estimated from time series of high-resolution observed data for a discrete number of dependency configurations. Parameter estimation is usually performed on a seasonal basis by considering

65 the dependency on the temporal scales of interests, and/or the dependency on the external pattern of precipitation (Olsson, 1998; Ormsbee, 1989; Güntner et al., 2001). The main drawback of empirical MRCs is the considerable number of parameters to be estimated, the large number of classes to be considered, and as a consequence, the lack of robustness of parameter estimates. In practice, some dependencies of the ECDFs are thus often ignored.

Besides empirical MRC models, analytical models aim to represent in a synthetic way the dependency of p_{01}, p_{10} and of the

70 distribution f_{W^+} to important factors of variability. Most analytical models have focused on the dependency on the temporal scale and precipitation intensity. For instance, a symmetric Beta distribution has been extensively used to model the distribution f_{W^+} (Menabde and Sivapalan, 2000). The single parameter α of the symmetric Beta distribution shows strong relationships with the temporal scale and the precipitation intensity, and can be modelled with simple scaling analytical laws (Molnar and Burlando, 2005; Paulson and Baxter, 2007; Rupp et al., 2009). To date, however, analytical models usually ignore the parameter

75 dependency on the external pattern of precipitation. An exception is the pattern-based MRC model presented by Hingray and Ben Haha (2005). Even though this pattern-based MRC model disregarded the important dependency on precipitation intensity, it was found to much better simulate a number of statistics relative to precipitation persistence and intermittency, statistics that are known to be difficult to reproduce with MRCs (e.g. Rupp et al., 2009; Paschalis et al., 2012, 2014; Müller and Haberlandt, 2018). The possibility to merge in a single and unified analytical scaling framework all the principal Γ dependencies is thus

80 expected to allow for a significant improvement of both its relevance and performance.

In the present work, we present an analytical MRC modelling framework that allows the cascade generator Γ to depend in a continuous way on temporal scales, intensity, and external pattern of precipitation. The following questions are considered:

- To what extent a continuous index of local precipitation asymmetry can describe the way the cascade generator Γ depends on the external pattern of precipitation?

85   – Is it possible to identify some scaling behaviour with respect to this asymmetry index and is it possible to propose an analytical relationship to model this scaling behaviour?

    – What is the added value of including such an asymmetry dependency in the cascade generator Γ, especially with regard to statistics related to precipitation persistence and intermittency?

One important application of disaggregation models is for locations where only coarse-resolution data are available. In this 90 case, the parameters of the model cannot be estimated from local data, as such data are missing, and are obtained with some regionalisation process based on data available from neighbouring and/or locations with similar precipitation regimes (e.g. Hingray et al., 2014). For such a work, analytical scaling MRCs are promising. They are very parsimonious which is expected to ease model regionalisation and increase model robustness.

However, introducing precipitation asymmetry dependence is at the expense of model parsimony. In this work, we thus 95 consider different MRC models, of different complexity, to find, if relevant, a compromise between model performance and parsimony. If the cascade generator is known to depict different types of scaling dependencies, not all are necessarily required to achieve fair model performance. Accounting for temporal scale dependence is widely considered to be beneficial. However, to our knowledge, the corresponding gain in performance is questionable (no improvement in Rupp et al. (2009) and loss of performance in Molnar and Burlando (2005)). Introducing dependence to intensity was conversely often found to significantly 100 improve it (e.g. Rupp et al., 2009; Paschalis et al., 2014).

An additional objective of the present work is to investigate the loss of performance obtained when the cascade generator Γ disregards the dependency on temporal scales. In particular, a model configuration that only accounts for the dependence on precipitation intensity and asymmetry is assessed.

The paper is structured as follows. In Sect. 2, we introduce a precipitation asymmetry index used to model the dependency 105 on asymmetry. Four different analytical MRC models are also presented in this section. They account for dependency on the temporal scale, precipitation intensity and/or precipitation asymmetry. The different models are used for the disaggregation of daily precipitation time series available for a large set of stations in Switzerland. Station locations and precipitation data are presented in Sect. 3. The models are evaluated on their ability to reproduce a number of characteristic statistics of precipitation at multiple temporal scales. Main performance evaluation results are presented in Sect. 4, while the interests of different model 110 components are discussed in Sect. 5. Section 6 concludes.

2   Methods

As mentioned previously, the cascade generator Γ used for the disaggregation of any precipitation amount R_0 is defined by the probabilities p_{01}, p_{10} and the distribution of W^+ denoted by f_{W^+}. In the following, f_{W^+} is modelled with a Beta distribution (McIntyre et al., 2016):

115   $$f_{W^+} = \frac{1}{B(\alpha_1,\alpha_2)} W^{+(\alpha_1-1)}(1-W^+)^{(\alpha_2-1)}, \tag{1}$$

where the Beta function $B(\alpha_1, \alpha_2)$ is a normalisation constant. The two parameters α_1 and α_2 are related to the mean and the variance of the distribution as follows:

$$E[W^+] = \frac{\alpha_1}{\alpha_1 + \alpha_2}, \tag{2}$$

and

120 $$Var[W^+] = \frac{\alpha_1 \alpha_2}{(\alpha_1 + \alpha_2)^2(\alpha_1 + \alpha_2 + 1)}. \tag{3}$$

Note that when $\alpha_1 = \alpha_2 = \alpha$, the distribution is symmetric,

$$E[W^+] = 0.5 \tag{4}$$

and

$$Var[W^+] = \frac{1}{4(2\alpha + 1)} \tag{5}$$

125 The MRCs compared in this study consider different ways to model their dependencies to the temporal scale, precipitation intensity, and precipitation asymmetry. Four models are compared:

- Model A accounts for the dependency on the temporal scale and precipitation intensity.

- Model B is a simplification of model A. It disregards the dependency on the temporal scale.

- Models A^+ and B^+ are refinements of models A and B, where the dependency to asymmetry is accounted for.

130 In the following, we describe the way the different models represent the scaling relationships for p_{01}, p_{10}, α_1 and α_2. We first present the MRC modelling framework of model A and the simplifications chosen for model B. Next, we introduce a precipitation asymmetry index further considered to account for the dependency of the cascade generator Γ on asymmetry. Finally, we describe how models A^+ and B^+ introduce this dependency.

2.1 MRC models without asymmetry: Models A and B

135 In models A and B, the dependency to precipitation asymmetry is disregarded and the distribution of the cascade generator is assumed to be symmetric. The probabilities p_{01} and p_{10} are thus assumed equal to each other and the distribution of the strictly positive breakdown coefficients, f_{W^+}, is modelled with a symmetric Beta distribution, i.e. $\alpha_1 = \alpha_2 = \alpha$.

The probabilities p_{01} and p_{10} are estimated from $p_x = 1 - p_{01} - p_{10}$, where p_x is the non-zero subdivision probability, i.e. the probability that the precipitation amount is split into two non-zero amounts. As illustrated with data from the Zurich station

140 in Figure 1a, p_x generally increases with the intensity of the precipitation amount to disaggregate and is expected to increase for coarser temporal scales. In model A, following Rupp et al. (2009), the scaling dependency of p_x on the temporal scale τ and precipitation intensity I is modelled as follows:

$$p_x(I, \tau) = \frac{1}{2}\left(1 + \text{erf}\left[\frac{\log(I) - \mu(\tau)}{\sqrt{2}\sigma(\tau)}\right]\right), \tag{6}$$

where erf is the error function defined as $\mathrm{erf}(x) = \frac{2}{\sqrt{\pi}} \int_0^x e^{-t^2}\,dt$ and where μ and σ are assumed to be linearly dependent on the logarithm of the temporal scale:

$$\mu(\tau) = a_\mu \log(\tau) + b_\mu, \tag{7}$$

$$\sigma(\tau) = a_\sigma \log(\tau) + b_\sigma. \tag{8}$$

In Model B, the dependency on the temporal scale is disregarded. In this case μ and σ are assumed constant and equation (6) simplifies to:

$$p_x(I) = \frac{1}{2}\left(1 + \mathrm{erf}\left[\frac{\log(I) - \mu}{\sqrt{2}\sigma}\right]\right). \tag{9}$$

The distribution f_{W^+} in models A and B is a symmetric Beta distribution. Its shape is defined by the value of its unique parameter α, which is related to the variance of W^+ via equation (5). For $\alpha = 1$, the probability density function (pdf) f_{W^+} is constant between 0 and 1, i.e. it corresponds to a uniform distribution. For $\alpha > 1$, the larger the value of α, the smaller the variance of W^+, the more the pdf is concentrated around its mean, 0.5. A roughly equal partition towards both sub-time steps becomes more likely in this case and leads to a stronger persistence of precipitation. For $\alpha < 1$, the smaller the value of α, the larger the variance of W^+, the more the pdf is concentrated close to 0 and 1, which leads to more variable and/or intermittent precipitation. In winter, for the Zurich station, Figure 1 shows that α increases ($Var[W^+]$ decreases) when precipitation intensity increases (Figure 1b) and α decreases ($Var[W^+]$ increases) when the temporal scale gets coarser (Figure 1b,c).

In model A, α is modelled as a function of precipitation intensity and temporal scale. Following Rupp et al. (2009), the model is the product of two functions of both variables, illustrated for Zurich data in Figure 1c and 1d respectively:

$$\alpha(\tau, I) = g(I) \cdot h(\tau), \tag{10}$$

where :

$$h(\tau) = \alpha_0 \cdot \tau^H, \tag{11}$$

and

$$\log[g(I)] = c_0 + c_1 \log(I) + c_2 [\log(I)]^2. \tag{12}$$

In model B, the dependency of α on the temporal scale is disregarded. The dependency on intensity is modelled with the following function:

$$\log(\alpha(I)) = \begin{cases} 0, & \text{if } I \leq I_0 \\ K\left[\log(I/I_0)\right]^2, & \text{if } I_0 < I \leq I_1 \\ K\left[\log(I_1/I_0)\right]^2, & \text{if } I > I_1 \end{cases} \tag{13}$$

where $I_0 = 0.1$ mm h^{-1} and $I_1 = 10$ mm h^{-1}, illustrated for Zurich data in Figure 1d. The distribution f_{W^+} is thus uniform for very low intensities. For large intensities, α is bounded to the value obtained for I_1. The higher the value for K, the higher

the curvature of the scaling function $\log(\alpha(I))$. Positive K values lead to higher α values for larger intensities (and vice versa). Models A and B have respectively nine ($a_\mu, b_\mu, a_\sigma, b_\sigma$ for p_x and $\alpha_0, H, c_0, c_1, c_2$ for f_{W+}) and three (μ, σ for p_x and K for f_{W+}) invariant parameters to be estimated.
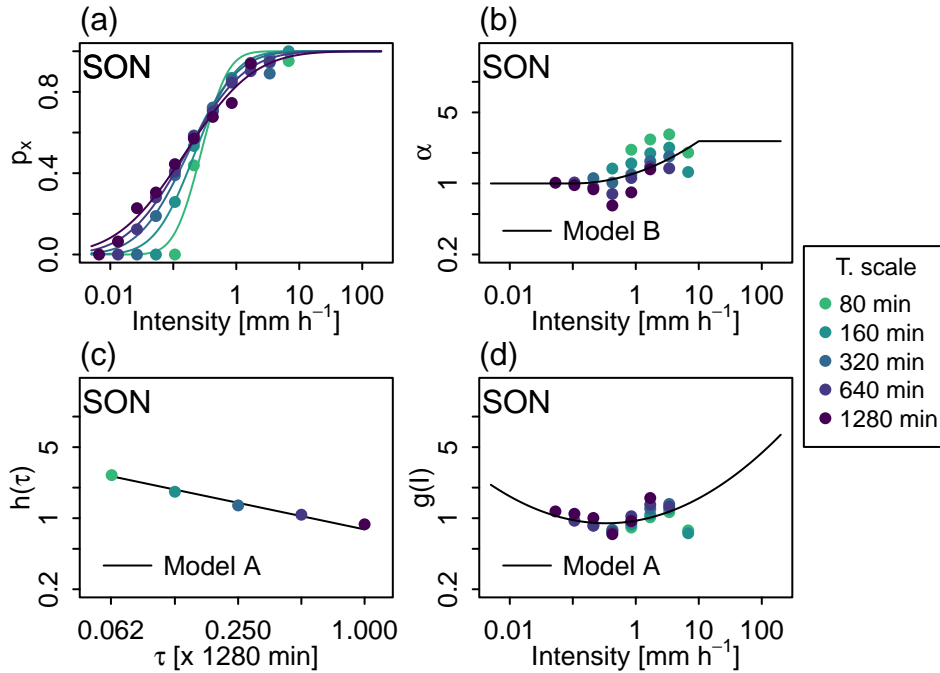
Figure 1. First row : two characteristics of the cascade generator Γ as a function of precipitation intensity I and temporal scale τ. (a) non-zero subdivisions probability p_x and (b) parameter α of the Beta distribution for f_{W+}. In panel (a), the different lines correspond to the different $p_x(I)$ models obtained for different scales according to the scaling model of model A (equation 6). In panel (b), the line corresponds to the scaling model for α in model B (equation 13). In both graphs, dots correspond to empirical estimates used for model fitting. They are obtained for different classes of intensity and different temporal scales. The colour indicates the temporal scale. Second row : the two scaling sub-models for α in model A. (c) model $h(\tau)$ (equation 11) and (d) model $g(I)$ (equation 12). In panel (c), dots correspond to empirical estimates of α for the different temporal scales (all intensities included). In panel (d), dots correspond to empirical estimates of the ratio $\alpha(I,\tau)/h(\tau)$ for different classes of intensity and different temporal scales. Data from the Zurich station, winter season.

2.2 An asymmetry index of precipitation sequences

175 To characterize the asymmetry of the precipitation sequence $\{R_{t-1}, R_t, R_{t+1}\}$, we introduce an asymmetry index Z_t as in Hingray and Ben Haha (2005). Z_t is defined as the shadow breakdown coefficient of the $\{R_{t-1}, R_t, R_{t+1}\}$ sequence. It is estimated from the two shadow precipitation amounts $R_1^* = R_{t-1} + 0.5R_t$ and $R_2^* = 0.5R_t + R_{t+1}$ that would be respectively obtained for the first and second halves of the $\{R_{t-1}, R_t, R_{t+1}\}$ sequence if R_t was split in half. Z_t thus reads:

$$Z_t = \frac{R_{t-1} + 0.5R_t}{R_{t-1} + R_t + R_{t+1}}. \tag{14}$$

180   While W is defined from the central precipitation and its subdivision amounts, Z_t is fully determined from the central and its
adjacent precipitation amounts. Z_t depends on the relative precipitation ratios R_{t-1}/R_t and R_{t+1}/R_t and varies from 0 to 1
as illustrated in Figure 2.
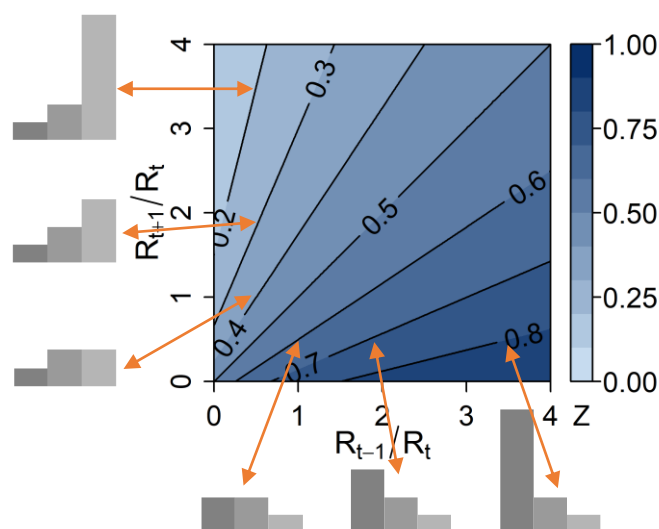
Figure 2. Asymmetry index Z_t of the $\{R_{t-1}, R_t, R_{t+1}\}$ precipitation sequence as a function of the two precipitation ratios R_{t-1}/R_t (x-axis) and R_{t+1}/R_t (y-axis).

The following points can be noticed:

–   A symmetric precipitation sequence, i.e. when $R_{t-1} = R_{t+1}$, leads to $Z_t = 0.5$ whatever the amount of precipitation on
185   the central time step.

–   For sequences with central precipitation amounts much larger than the adjacent ones, Z_t is close to 0.5.

– $Z_t < 0.5$ indicates an "increasing" or "right valley" sequence, i.e. a sequence where $R_{t-1} < R_{t+1}$, while $Z_t > 0.5$ indicates a "decreasing" or "left valley" sequence ($R_{t-1} > R_{t+1}$).

–   The Z_t asymmetry index characterizes in a continuous way the intensity of the asymmetry; different "decreasing" pre-
190   cipitation sequences will have different Z_t values depending on the "steepness" of the decrease. The larger the deviation
from 0.5, the larger the asymmetry.

– Z_t values close to 0 indicate sequences with very little rain on the first two time steps when compared to the last one
(very steep "ascending" sequences), whereas Z_t values close to 1 indicate sequences with very little rain on the two last
time steps when compared to the first one (very steep "descending" sequences).

2.3 ECDF dependency on precipitation asymmetry and scaling models

Figure 3a shows the ECDFs of observed weights W obtained for the Zurich station for 10 classes of precipitation asymmetry index, defined as $G_l^Z = \{W_t | Z_t \in (0.1(l-1), 0.1l]\}$, for $l = 1, \ldots, 10$. As expected, the ECDF depends a lot on the asymmetry class. The lower the value of Z_t (i.e. corresponding to very steep ascending external patterns), the higher the value of p_{01} and the lower the value of p_{10}. In other words, the higher the probability that all the R_t precipitation amount is attributed to the second subdivision and the lower the probability that all R_t is attributed to the first subdivision. The exact opposite happens for high values of Z_t (i.e. values corresponding to very steep descending external patterns).

The asymmetry of the precipitation sequence directly translates to an asymmetry of the ECDF of W, namely to an asymmetry between p_{01} and p_{10} and to an asymmetry of the distribution f_{W+}. As shown in the following, the asymmetry of ECDF significantly depends on the value of the asymmetry index z. For clarity, the temporal index t is omitted hereafter.

To quantify the asymmetry between p_{01} and p_{10}, we introduce the probability asymmetry ratio, φ, defined as:

$$\varphi = \frac{p_{01}}{p_{10} + p_{01}} = \frac{p_{01}}{1 - p_x}. \tag{15}$$

For φ values close to 0.5, the asymmetry between p_{10} and p_{01} is small. The case $\varphi = 0.5$ corresponds to the symmetric case, i.e. $p_{10} = p_{01}$. The most asymmetrical configurations are obtained when $\varphi = 0$ or $\varphi = 1$. The case $\varphi = 0$ (resp. $\varphi = 1$) corresponds to $p_{01} = 0$ and $p_{10} = 1 - p_x$ (resp. $p_{01} = 1 - p_x$ and $p_{10} = 0$). The relationship between φ and z is illustrated in Figure 3b. As expected, when z increases, φ decreases. The $\varphi(z)$ relationship is found to be roughly similar for all Swiss stations (results not shown) and can be modelled with an error function as follows:

$$\varphi(z) = \frac{1}{2}\left(1 + \operatorname{erf}\left(\frac{0.5 - z}{\nu\sqrt{2}}\right)\right), \tag{16}$$

where the single parameter ν is related to the strength of the $\varphi(z)$ relationship around the pivot point ($z = 0.5$, $\varphi = 0.5$). The strength is found to depend on the station and on the season. It is for instance slightly higher in winter than in summer for Zurich station.

For asymmetric precipitation sequences, the distribution f_{W+} is also expected to be asymmetric. In particular, the mean of the distribution is expected to differ from 0.5. This is illustrated in Figure 3c for Zurich observation data, where the mean of W^+, denoted by m, is estimated for different classes of z. As expected, the lower the value of z, the lower the value of the mean. In terms of precipitation dynamics, this reflects the fact that in an ascending precipitation sequence, the amount of precipitation tends to be smaller in the first time subdivision than in the second one. The reverse is true in the case of a descending sequence. The $m(z)$ relationship highlighted in Figure 3c is found to be roughly linear for all Swiss stations (results not shown) and can be modelled as:

$$m(z) = \lambda\left(z - \frac{1}{2}\right) + \frac{1}{2}. \tag{17}$$

The model is centred on the pivot point ($z = 0.5$, $m = 0.5$). Its unique parameter λ corresponds to the slope of this linear function and indicates the strength of the dependency on precipitation asymmetry z. The strength is also found to depend on the season and site.

In models A^+ and B^+ described in the following section, the dependency of the cascade generator Γ on precipitation asymmetry is accounted for with the help of the scaling models $\varphi(z)$ and $m(z)$. Both scaling models have one single invariant parameter to estimate.
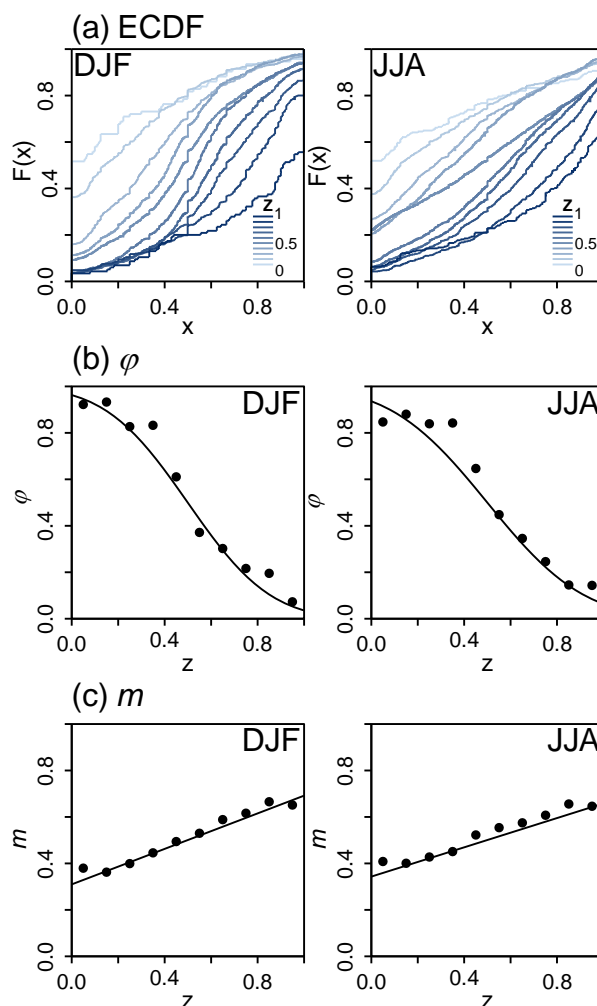
Figure 3. Statistical characteristics of the breakdown coefficients W as a function of the asymmetry index z for Zurich station in winter (DJF, left column) and summer (JJA, right column). (a) ECDFs of W for 10 classes of z. (b) Dry probability asymmetry ratio φ as a function of z. The estimates φ obtained for different classes of z are indicated with black dots and the fitted model $\varphi(z)$ with a plain black line. (c) Estimated mean of W^+ as a function of z. Empirical means are indicated with black dots and the fitted model $m(z)$ with a plain black line.

2.4 MRC models with asymmetry : Models A^+ and B^+

The introduction of asymmetry in model A, leading to model A^+, is described hereafter. In model A^+, the non-zero subdivision probability p_x is obtained for I and τ as in model A with the scaling model $p_x(I, \tau)$ presented in Sect. 2.1 (see equation 6).

Contrary to model A, probabilities p_{01} and p_{10} can be different and are obtained from the definition (15) of the probability asymmetry ratio $\varphi(z)$ as follows:

$$p_{01} = \varphi(z)\,(1 - p_x)\,, \tag{18}$$

$$p_{10} = (1 - \varphi(z))\,(1 - p_x)\,. \tag{19}$$

In model A$^+$, the Beta distribution f_{W^+} can be asymmetric and its two parameters can be related to $E[W^+]$ and $Var[W^+]$ from equations (4) and (5) as follows:

$$\alpha_1 = \left(\frac{E[W^+]\,(1 - E[W^+])}{Var[W^+]} - 1 \right) E[W^+]\,, \tag{20}$$

$$\alpha_2 = \left(\frac{E[W^+]\,(1 - E[W^+])}{Var[W^+]} - 1 \right) (1 - E[W^+])\,. \tag{21}$$

In model A$^+$, we obtain $E[W^+]$ from the scaling model $m(z)$ of equation (17) and $Var[W^+]$ is assumed to be the same as in model A, i.e. in a configuration where the distribution is assumed symmetric. In practice, $Var[W^+]$ is thus simply derived from the value of α obtained with the scaling model $\alpha(I,\tau)$ of model A as follows: $Var[W^+] = 1/(4\,(2\alpha(I,\tau)+1))$. The parameters α_1 and α_2 are then simply derived from these representations of $E[W^+]$ and $Var[W^+]$.

Model B$^+$ is derived from model B in the same way. The probabilities p_{01} and p_{10} are obtained from equations (18) and (19) with the scaling model $p_x(I)$ of equation (9). α_1 and α_2 are obtained from equations (20) and (21) where $E[W^+]$ and $Var[W^+]$ are obtained respectively from the model $m(z)$ and from $1/(4\,(2\alpha(I)+1))$.

2.5 Estimation of scaling models

Table 1 summarizes the dependencies of each MRC model to either temporal scale, intensity and/or asymmetry and indicates the parameters to be estimated for the corresponding scaling models.

Whatever the MRC model, the estimation of the different parameters required for the scaling model for p_x is independent of those related to α. The estimation of the scaling sub-model for the probability asymmetry index φ and for the mean m of the distribution f_{W^+} is also independent of the estimation of the scaling models for the dependency to intensity/temporal scale. In all cases, the estimation is also sequential: in a first step, the empirical value of the variable of interest (e.g. p_x, α, φ or m) is calculated for different classes of disaggregation configuration (e.g. different temporal scales, or different classes of intensity, or different classes of asymmetry index) and in a second step, the relevant scaling model is fitted to those empirical values by the method of least square errors.

This is illustrated in panels (b) and (c) of Figure 3 for the asymmetry scaling model $\varphi(z)$ and $m(z)$. The models of equations 16 and 17 are fitted (the plain black lines) on the empirical values of φ and m obtained for different asymmetry index classes (black dots). Empirical values of φ and m are calculated for each z-index class by ignoring the intensity class and temporal scale. Estimation is also made on a seasonal basis. The estimation process for the parameters of the other scaling models is similar. It is described in detail for all models in Appendix A. An example of model fit is given in Figure 1a, c and d (plain lines) for the scaling models $p_x(I,\tau)$, $g(I)$ and $h(\tau)$ used in model A. For the scaling model $\alpha(I)$ used in model B, an example is given in Figure 1b.

Table 1. The 4 models compared and the parameters to be estimated for the scaling sub-models accounted for. The - symbol denotes a configuration where the scaling dependency is disregarded. The total number of parameters is given in column "Nb. of params".

Model	Nb. of params	p_x or (p_{10} and p_{01})			f_{W+} (α only or α_1 and α_2)		
		Intensity	Temporal scale	Asymmetry	Intensity	Temporal scale	Asymmetry
A	9	$p_x(I,\tau) \rightarrow a_\mu, b_\mu, a_\sigma, b_\sigma$		-	$\alpha(\tau,I) \rightarrow c_0, c_1, c_2, \alpha_0, H$		-
A$^+$	11	$p_x(I,\tau) \rightarrow a_\mu, b_\mu, a_\sigma, b_\sigma$		$\varphi(z) \rightarrow \nu$	$\alpha(\tau,I) \rightarrow c_0, c_1, c_2, \alpha_0, H$		$m(z) \rightarrow \lambda$
B	3	$p_x(I) \rightarrow \mu, \sigma$	-	-	$\alpha(I) \rightarrow K$	-	-
B$^+$	5	$p_x(I) \rightarrow \mu, \sigma$	-	$\varphi(z) \rightarrow \nu$	$\alpha(I) \rightarrow K$	-	$m(z) \rightarrow \lambda$

265   Precipitation data aggregated at six temporal resolutions are considered for model estimation (40, 80, 160, 320, 640, and 1280 min). 40-minute precipitation data are obtained from the 10-minute time series available for the stations. The 40-minute time series are aggregated to 80-minute time series to calculate the observed breakdown coefficients W using non-overlapping adjacent pairs of precipitation amounts for this cascade level. The aggregation procedure is repeated until the time series reaches the temporal resolution of 1280 minutes. These different series are used for the estimation of the breakdown coefficients relative

270 to each temporal scale and are also used as a reference for the evaluation of the disaggregation models (see Sect. 2.6).

     Note that the 1280-minute aggregated temporal scale does not correspond to the daily resolution of 1440 minutes. Following Molnar and Burlando (2005), the first and last 80-minute records of each day were thus discarded from the initial observed times series before aggregations. The resulting time series, with truncated days of 21.3 hours, was used as a reference "daily" time series for model estimation and evaluation.

275   As reported in previous works, the precipitation measurement resolution, defined by the precipitation tipping bucket of automatic stations, 0.1 mm here, is very likely to introduce artefacts and/or biases in different statistical characteristics of precipitation at fine temporal scales, especially sub-hourly ones and can impact the empirical distributions of the breakdown coefficients W (e.g. Olsson, 1998; Rupp et al., 2009; Paschalis et al., 2012). Following previous works, the breakdown coefficients W obtained from precipitation amounts below a given precipitation threshold were discarded for the present study. A

280 threshold of 0.8 mm is applied for the estimation of α in all models, and for the estimation of p_x in models B and B$^+$ (see Sect. 5.1 for further discussion on this issue).

2.6   Experimental setup

The 10-minute observational records aggregated to the resolution of 1280 minutes are disaggregated back to the 40-minute resolution using models A, B, A$^+$ and B$^+$. Since models are stochastic, the disaggregation is performed 30 times for each

285 model.

     The performance of a given model is evaluated by its ability to reproduce standard statistical metrics of precipitation, such as the standard deviation of precipitation amounts, the probability of precipitation occurrence, and return levels of maximum precipitation amounts for given return periods. In addition, the temporal autocorrelation, wet-dry transition probabilities and the

duration of wet and dry spells are used to assess the ability of the models to reproduce the temporal persistence of precipitation.
290   Evaluations are carried out on a seasonal basis for all available stations and for all temporal scales involved in the generation
process (i.e. 40 to 640 minutes).

Different evaluation criteria are used. For most evaluation metrics, the variability between generated scenarios is small to
very small. In this case, the evaluation criterion is the absolute error between the simulated and the observed metric, averaged
over the different scenarios (and possibly temporal scales and seasons). To assess the performance of a given model across
295   multiple sites, single-site performances are averaged over the different stations. We refer to this performance criterion as the
Mean Absolute Error (MAE). For some metrics, the percentage absolute relative error is considered (dividing for each station,
season, temporal scale, the absolute error by the observed value of the metric), giving the Mean Absolute Percentage Error
(MAPE, Hyndman and Koehler, 2006).

For precipitation maxima, the variability between scenarios is often large. In this case, we apply the CASE evaluation
300   framework proposed by Bennett et al. (2018) for which at-site model performances are categorized as "good", "fair" and "bad".
For a single metric at a given site, 90% and 99.7% probability limits are obtained from the set of simulated metrics and are
confronted with the observed metric. Then, the performance is categorized as:

  – "good", if the observed metric is inside 90% limits of simulated metrics,

  – "fair", if the observed metric is outside of 90% limits of simulated metrics but within the 99.7% limits of simulated
305   metrics or absolute relative difference between the observed metric and the average simulated metrics is 5% or less, and,

  – "bad", otherwise.

To assess the performance of a given model across multiple sites, single-site performances are summarized as percentages of
"good", "fair" and "bad" cases among sites and seasons. The variables evaluated here are the return levels obtained for 5 and
20 years return periods.

3 Application to Swiss data

The four models are applied to 81 stations of the Swiss meteorological observation network, a relatively dense network, with
high-quality observational data (Figure 4). The stations have at least 20 years of data available through the period 1980-2020
and use tipping bucket rain gauges with a sampling resolution of 10 minutes and tip volume of 0.1 mm. Switzerland has a
complex topography, with 60% of the territory covered by the Alps. Together with the Swiss Plateau and Jura mountains on the
315   north, they are the main features of the landscape. The complex topography induces very different weather and precipitation
regimes as described in the precipitation climatology for the European Alps of Frei and Schär (1998). For instance, the main
topographic slopes at the rim are responsible for enhanced precipitation and associated rain-shadowing of inner-Alpine sectors.
The Swiss Plateau tends to be sheltered by the Jura mountains, resulting in less precipitation from northwest fronts during
winter than the Jura mountains (Baeriswyl and Rebetez, 1997).
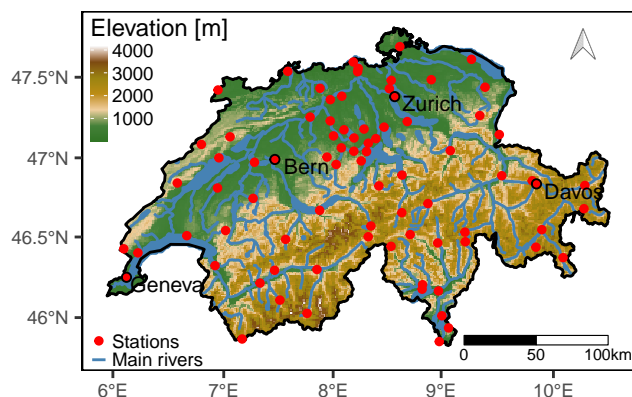
Figure 4. Map of Switzerland and gauge locations.

320   If large precipitation amounts can be observed during winter and spring due to long stratiform and orographic precipitation events, intense precipitation events are often observed in summer and fall due to the topographically triggered convective events (Frei and Schär, 1998). Mediterranean cyclonic activity in autumn brings heavy precipitation in the region of Ticino, in the south of Switzerland, making autumn the main precipitation season in this region (Molnar and Burlando, 2008).

4   Results

325 We first focus on results obtained for the target 40-minute temporal resolution, namely for a set of standard statistics (Sect. 4.1) and for 5- and 20-year return levels of annual maxima (Sect. 4.2). Next, in Sect. 4.3 we present how results vary for intermediate disaggregation temporal resolutions and for the different seasons.

4.1   Standard statistics

Simulated values obtained for a set of standard statistics at a resolution of 40 minutes are confronted to observed ones in Figure
330 5. For standard deviation and proportion of wet 40-minute time steps, results are satisfying whatever the model. Slightly better results (i.e. smaller MAE values) are obtained with models B and B^+ for standard deviation (Figure 5a) and with models A and A^+ for the proportion of wet steps (Figure 5b).

    Differences between models are more important for statistics related to precipitation persistence and intermittency. The best-performing model depends on the statistic but, whatever the statistic, the performance of the model is always drastically
335 improved when precipitation asymmetry is accounted for (see model A^+ vs model A, and model B^+ vs model B). At a 40-minute resolution, this is illustrated with results obtained for the wet/dry transition probability, lag-1 autocorrelation, and mean duration of wet spells in panels (c), (d), and (e) of Figure 5 respectively. For all stations and all seasons, the large over- or under-estimation obtained with models A and B is largely reduced and even tends to disappear when asymmetry is accounted for (models A^+ and B^+). In the same manner, much better results are obtained for all other similar statistics and all other

340 temporal scales, as indicated by the results obtained for lag-2 autocorrelation, mean duration of dry spell and all the other wet/dry transitions probabilities (dry/dry; dry/wet; wet/wet) provided in the SM (see Figure S3, S4 and S5).

Some differences are also noticed depending on whether or not the dependency on the temporal scale is taken into account (i.e. model B vs model A, and model B^+ vs model A^+). While these differences are sometimes non-negligible, they are much smaller than the obtained differences depending on whether or not the dependency on the asymmetry is included. For example,

345 at the 40-minute resolution, the observed autocorrelation coefficients are better reproduced with a dependency on the temporal scale (Figure 5d for lag-1 and Figure S3 for lag-2 in the SM). For durations of wet and dry spells and the different wet/dry transitions probabilities, the consideration of dependency on the temporal scale has a limited influence (see panels (c) and (f) of Figure 5 for the duration of wet spell and wet/dry transition probability, and Figure S4, S5 of SM for other statistics).
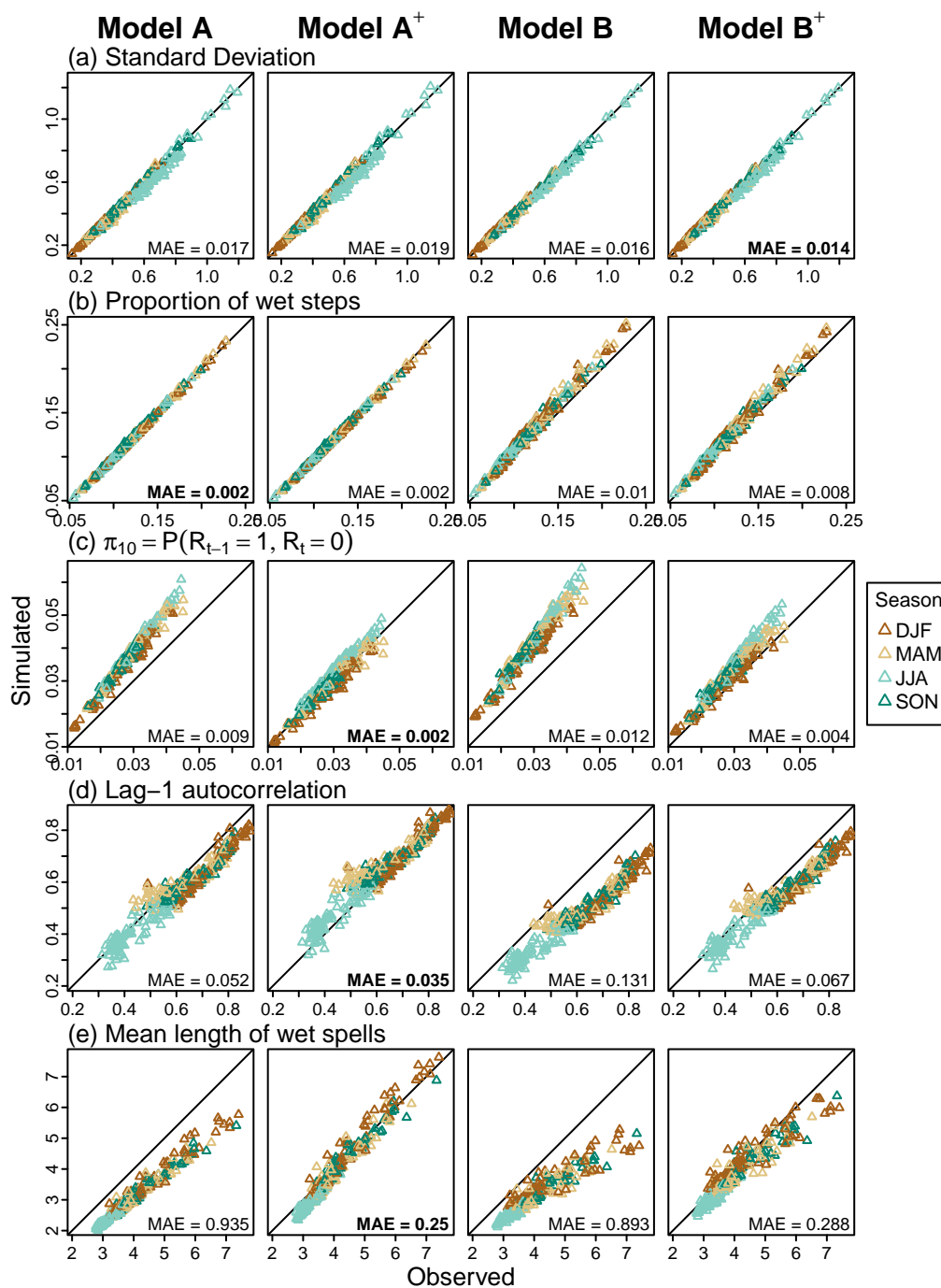
Figure 5. Observed versus simulated statistics for each considered model at a 40-minute temporal resolution for different metrics. Each triangle represents a site and a season. The triangles for the simulated metrics correspond to the median of the 30 statistics obtained from the corresponding 30 simulated scenarios. MAE values over all sites and seasons are indicated in the bottom-right corner, the lowest MAE obtained over the four models being indicated in bold. Pearson's autocorrelation coefficients are estimated using the function `acf` implemented in R, R Core Team (2022).

4.2 5- and 20-years return levels

350 The ability of the models to simulate relevant return levels for the 5- and 20-year return periods at the 40-minute temporal resolution is presented in Figure 6. The percentages of station/season configurations corresponding to the "good", "fair" and "poor" CASE criteria are summarized with the horizontal green/yellow/red bar, respectively, in each graph.

Results are very similar from one model to the other. The percentage of sites with "good" performance is slightly higher for models B and B$^+$ but MAPE values are very similar for all models. Contrary to most of the other considered metrics, the 355 consideration of asymmetry has almost no influence here.

All models are able to reproduce the large variety of 5- and 20-year return levels observed in Switzerland between sites and seasons. They also all perform rather well for both return periods. For most sites and seasons, however, return levels are slightly underestimated. At the 40-minute resolution, the underestimation is stronger in spring and summer for some sites (Figure 7). This point will be further discussed in Sect. 5.5.
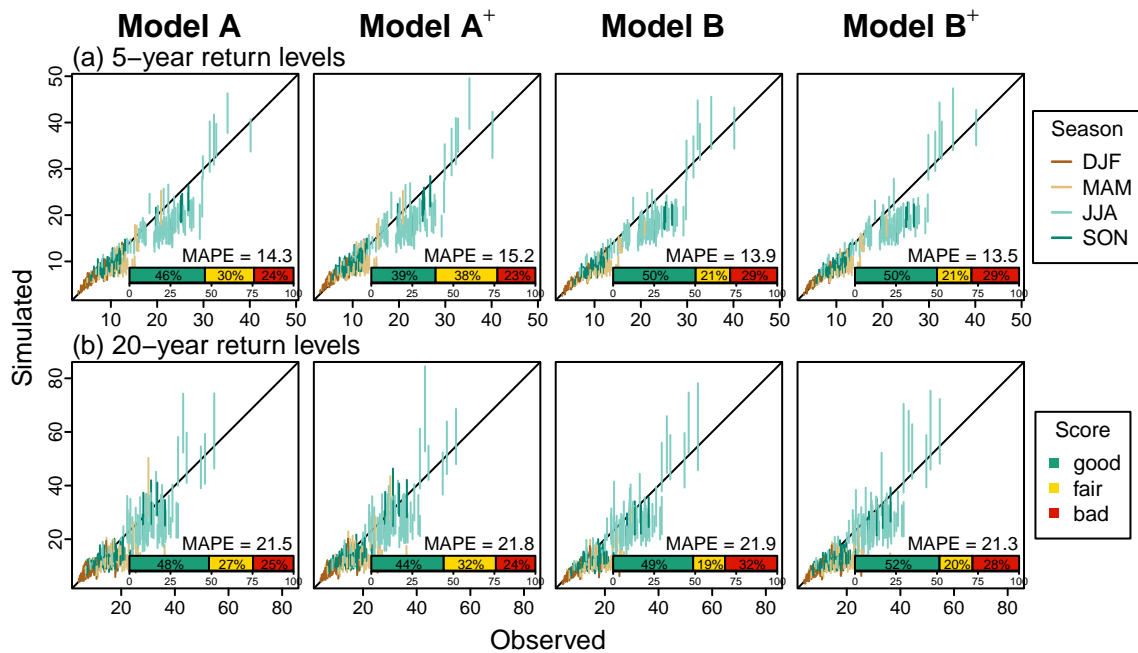
Figure 6. Observed versus simulated return levels at the 40-minute temporal resolution for (a) 5-year and (b) 20-year return periods, for each model and at each site. Vertical bands indicate the 90% CI limits obtained from the 30 simulated time series for each station and each season (one colour by season). Horizontal coloured bars indicate the percentage of "good", "fair", and "poor" performance as assessed by the CASE framework for all sites and seasons (81 × 4 = 324 cases). The return levels are estimated empirically using the Gringorten formula (Gringorten, 1963).

4.3 Intermediate temporal scales and dependency to seasons

360

Figure 7 presents the performance of each model for the reproduction of the lag-1 autocorrelation, mean length of wet spells, 5-year and 20-year return levels at different temporal resolutions. Clearly, for almost all statistics, the performances depend on the temporal resolution. For the intermediate disaggregation resolutions, the best-performing models are not necessarily the same as those found at a 40-minute resolution. For instance, between models A and B, in regard to the reproduction of the

365 lag-1 autocorrelation, the best model at a 40-minute resolution is model A, while model B is the best model at 160-minute and coarser resolutions. For the mean length of wet (and dry) spells and for 5- and 20-year return levels, models A and B provide similar performance for 40-minute although model B tends to perform better at 160 minutes and at coarser resolutions.

At 40-minute resolution, accounting for asymmetry significantly improves the reproduction of all statistics related to precipitation persistence and intermittency, but does not influence the reproduction of standard deviation, wet step probability, and

370 return levels. Similar results are obtained for the intermediate temporal resolutions.

As already mentioned previously, results can also depend on the season. Results for spring and summer are often similar and contrast with the results obtained in winter and autumn (see Figure 7).
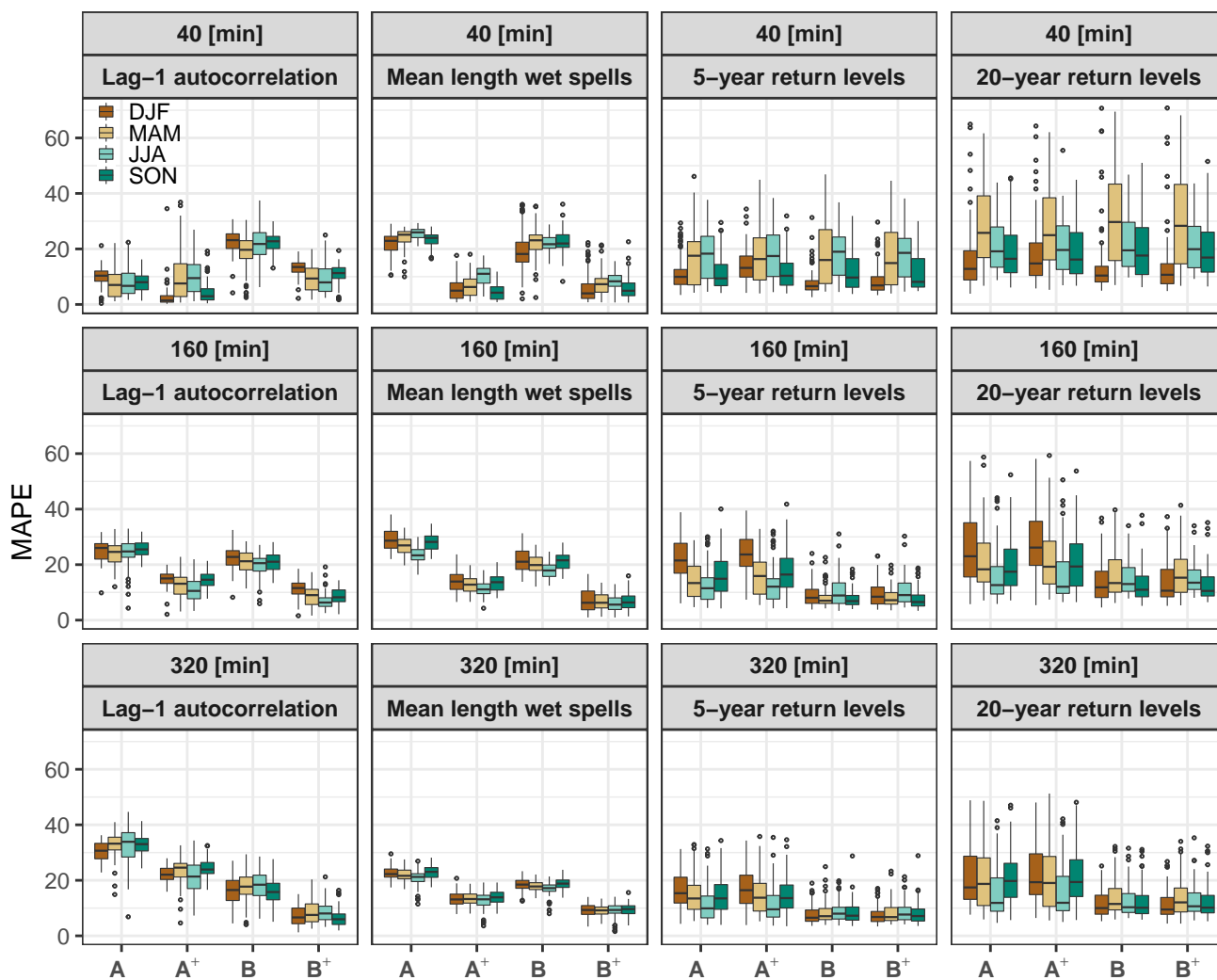
Figure 7. Mean Absolute Percentage Error (MAPE) as a function of the temporal aggregation level and season for lag-1 autocorrelation, mean length of wet spells, 5-year and 20-year return levels. Each boxplot summarizes the single site performances obtained for the 81 stations.

5 Discussion

5.1 Scaling MRC parameters with temporal scales

375 As highlighted in many previous works, the distribution of the breakdown coefficients W^+ depends on the temporal scale, precipitation intensity, precipitation asymmetry and possibly other factors. To our knowledge, and with the exception of the pattern-based MRC model presented in Hingray and Ben Haha (2005), all analytical MRC developments have focused on temporal scale and intensity dependencies.

According to the results shown in Sect. 4, the dependence on the temporal scale and its added value are not as pronounced as

380 usually considered. In the present study, model A, which is the model considered by Rupp et al. (2009), and later by Paschalis et al. (2014), includes the dependency on the temporal scale and precipitation intensity. Model B, a simplification of model A, disregards temporal scale dependency. Besides the fact that it increases the number of parameters to be estimated (six additional parameters), model A is found to have similar performances to model B and even worse for coarse temporal scales. Note that Molnar and Burlando (2005) and Rupp et al. (2009) also show this limited advantage of the temporal scale dependency.

385 Two issues must be put in perspective with the preceding statements. The first one is related to the recording precision, which induces a relatively high frequency of $W = 1/2, 1/3, 2/3$, and to a lesser extent of $W = 1/4$ and $3/4$. This precision artefact is actually detrimental for a relevant estimation of the cascade generator Γ characteristics for small temporal scales and low intensities (not for moderate to high intensities, see, e.g. Olsson, 1998; Rupp et al., 2009; Paschalis et al., 2012). Rupp et al. (2009) suggested that some of the dependency on intensity was the result of this artefact precision. We argue that a large part

390 of the dependency on the temporal scale is also a result of this precision artefact. This is clearly shown here concerning the probability $p_x(I)$. As illustrated in Figure 1a, the $p_x(I)$ relationship for the Zurich station differs from one temporal scale to the other. The difference between the curves, which is mainly observed for small to very small intensities, depends a lot on the low precipitation threshold considered for selecting precipitation data (not shown). The differences between the curves almost disappear when precipitation amounts smaller than 0.8 mm are removed from the analysis (see Figure S2 in the SM for the

395 Zurich station). Without the small precipitation amounts, the scaling model for $p_x(I)$ does not depend on the temporal scale anymore and motivates the simplification of model B considered here. This issue also calls for the development of a robust assessment framework (to be defined) that would be able to disentangle, if existent, the genuine dependence on the temporal scale from the one induced by the precision artefact.

Another issue concerns the parameter α of the distribution f_{W^+}. For this parameter, the dependence on the temporal scale

400 is poorly understood. For Zurich, rather large deviations are obtained between modelled and empirical estimates whether this dependence is taken into account (model A, see scaled parameter $g(I)$ in Figure 1d) or not (model B, see Figure 1b). Deviations are mainly observed for large intensities in model A and for moderate intensities in model B. The temporal scale dependency assumption also seems to be detrimental for the disaggregation of large precipitation amounts. In all cases, none of the two models A and B are fully satisfying for representing α, similar results being obtained for all other stations considered in this

405 work. The dependency on the temporal scale needs to be better characterized in future works, along with alternative scaling models.

5.2 Scaling MRC parameters with precipitation asymmetry

The statistics related to precipitation persistence have always been found to be significantly underestimated by analytical MRC models (e.g. Hingray and Ben Haha, 2005; Rupp et al., 2009; Paschalis et al., 2012). Paschalis et al. (2014) actually
410 suggest that analytical MRCs, by construction based on a symmetric cascade generator, are unable to account for the multiscale autocorrelation structure of precipitation. The results shown in Hingray and Ben Haha (2005) indicate that this issue could be at least partly fixed when the precipitation asymmetry is accounted for in the model. These insights are thus confirmed with the present work, for a large variety of climate contexts found in Switzerland and for all seasons.

The dependence on precipitation asymmetry, acknowledged for a long time, was never accounted for in a fully analytical
415 MRC framework. This study fills this methodological gap. We show that the dependency on the asymmetry can be modelled with a two-part analytical scaling sub-model, where the dry probability asymmetry ratio φ and the mean m of the positive breakdown coefficients distribution f_{W+} depend on the precipitation asymmetry index z. For Swiss stations, the dependence of the cascade generator properties on precipitation asymmetry seems to be much larger than that on temporal scales. The added value of introducing precipitation asymmetry in the model is clear: all statistics relative to precipitation persistence are
420 much better reproduced, whatever the station, the season, and the temporal scale.

5.3 Spatial variability of parameters and potential for a regional MRC model

In order to apply a MRC model in locations where only daily data are available, the possibility to develop a robust regional model for model parameters is necessary. The smaller the number of parameters, the more robust and easier the regionalisation is expected to be. In this regard, model B^+ (5 parameters) is likely to be much more appropriate for regionalisation than model
425 A^+ (11 parameters).

Another important factor that can jeopardize the success of parameter regionalisation is the spatial variability of parameters. In case of no evident relationship to some geographical features (e.g. topography), smooth spatial variations of parameters often help achieve robust regionalisation. The spatial variability of the five parameters of model B^+ is shown in Figure 8 where maps of estimates for μ, σ, K, ν and λ are presented for each season. Regardless of the parameter and throughout all seasons,
430 the regional coherency is rather impressive. All parameters present significant spatial variability, reflecting the large variety of regional climates in Switzerland, nevertheless, the spatial variations are very smooth at sub-regional scales and from one region to the other. These results give increased confidence in the relevance of estimates and in the robustness of the model. They also suggest that a relevant regional model will be possible for all parameters, enabling the temporal disaggregation of coarse-resolution precipitation data anywhere in Switzerland. The performance of such a regional MRC model will be further
435 investigated in future works.

5.4 Seasonal variability of parameters

Additionally, the maps presented in Figure 8 depict the seasonal variations of the various parameters. As already shown in previous works (e.g. Molnar and Burlando, 2005), the season is actually a much larger factor of variability than the location.

The contrast between winter and summer is particularly marked. Whatever the parameter, the values for spring and autumn are

440   similar to each other. This seasonality reflects the different types of rainfall events throughout the year, with more stratiform events in winter, more convective ones in summer, and mixed types in intermediate seasons. Stratiform events are generally persistent in time and with a large spatial extent, contrary to convective events which are often localized and with a short duration. The partition of any precipitation amount in two parts is thus expected to be smoother in winter, with more frequent partitions of similar rainfall amounts on the two subdivisions, and more dependency on the external precipitation pattern. This is

445   reflected by higher p_x values, higher α values as well as higher sensitivity to precipitation asymmetry. This is also shown by the values of all scaling parameters in winter: lower values of μ and σ for the intermittency probability scaling sub-model, higher value of K for the no-dry subdivision scaling sub-model, lower value of ν and higher value of λ for the asymmetry scaling sub-models. As suggested by Rupp et al. (2009), an alternative to the seasonal stratification could consist of a parameterization conditional on the type of precipitation events, especially for intermediate seasons where different types of events are observed.
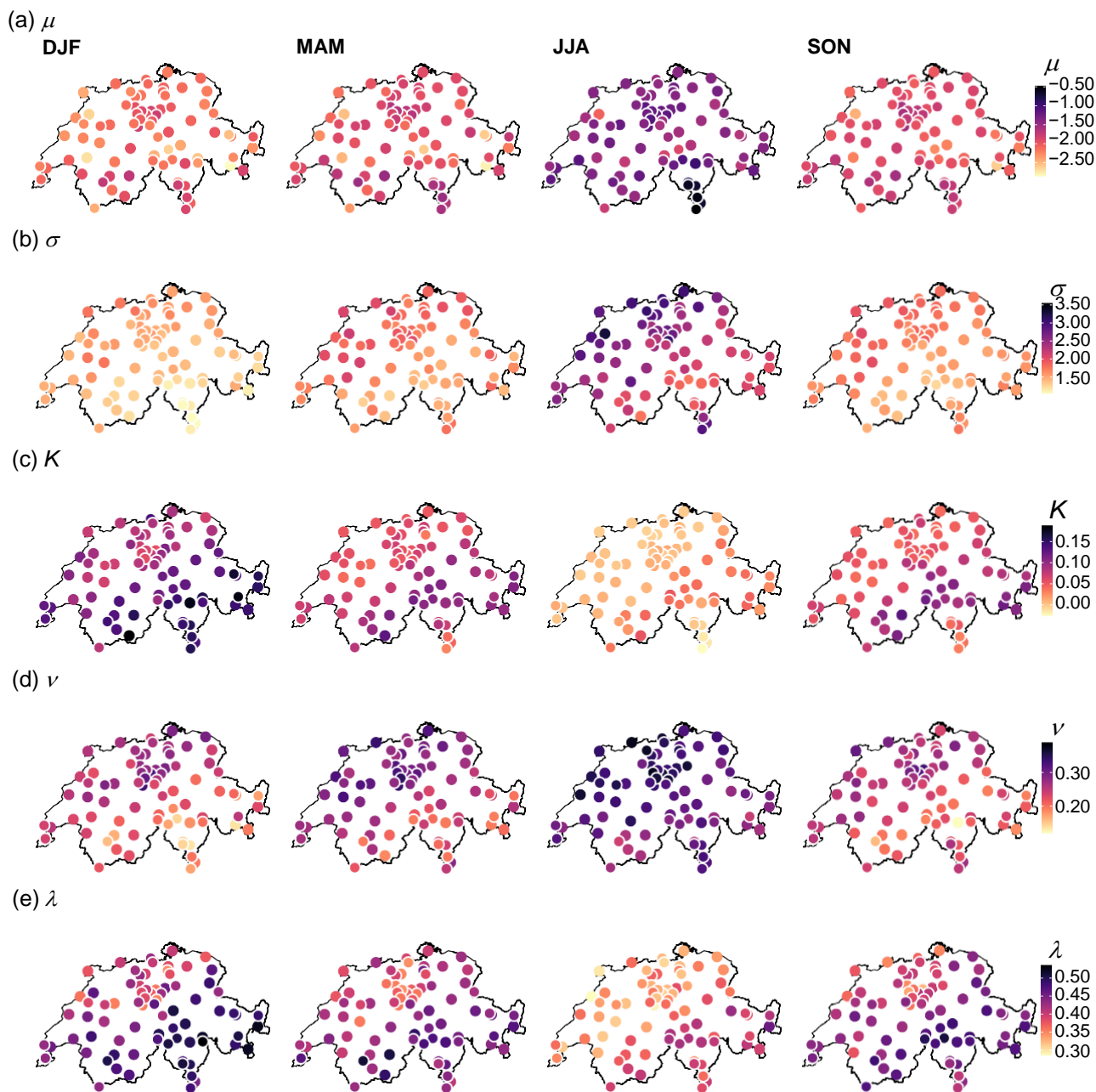
Figure 8. Maps of Switzerland showing spatial and seasonal variations of the estimated parameters for model B$^+$. Each row corresponds to one parameter of the model. Parameters representing the relationship between intermittency and intensity are those of the equation (9): (a) μ and (b) σ. (c) Parameter K, equation (13), related to the dependency of the distribution of positive weights, f_{W+}, on the precipitation intensity and finally the parameters ν and λ in (d) and (e), respectively, hold the dependency of the cascade weights on the precipitation asymmetry through equation (16) and equation (17). The colour of the circle indicates the value of the parameter estimate for the respective station and season.

5.5 Asymptotic assumption of no-dry subdivisions probability for high intensities

An opportunity for model improvement concerns the scaling sub-model for the no-dry subdivisions probability p_x. As shown in Sect. 4.2, all the models tend to underestimate spring and summer extreme events on some sites. Figure 9a shows that, for model B, this principally occurs in northern Switzerland for spring and summer seasons. Very similar maps are obtained for the other models (not shown). A plausible explanation is that the model used for p_x is not valid for very large intensities.

Following previous works, p_x is assumed to be related to precipitation intensity via the erf function of equation (6). By construction, for large precipitation intensities, this scaling model has an asymptotic value of one, and p_{01} and p_{10} tend to zero. In other words, very large precipitation amounts are systematically divided into two non-zero parts. However, the probability p_x has no reason to tend to 1, especially at coarse temporal scales (see illustration in Figure S2 in the SM). For instance, large daily precipitation amounts in summer can result from intense convective events with short duration (less than an hour). In this case, the daily amount must not be subdivided nor spread over multiple high-resolution time steps. The breakdown coefficients for such events are either 0/1 or 1/0 and the probability to have the 1/1 configuration is expected to be possible for high resolutions only. When p_x is overestimated for large intensities, the 1/1 configurations (no-dry subdivisions) are thus over-represented and lead to an underestimation of extreme values.

The misrepresentation of p_x for large intensities is illustrated with the mean deviation obtained between modelled and empirical p_x values for intensities larger than $1 \, \mathrm{mm \, h^{-1}}$ in Figure 9b. Whatever the season, the spatial pattern of these deviations fits very well with that obtained for the underestimation of the 5-year return level shown in Figure 9a. The larger the deviation, the worse the underestimation. Relaxing the current asymptotic assumption for the p_x model may improve the simulation of extremes.
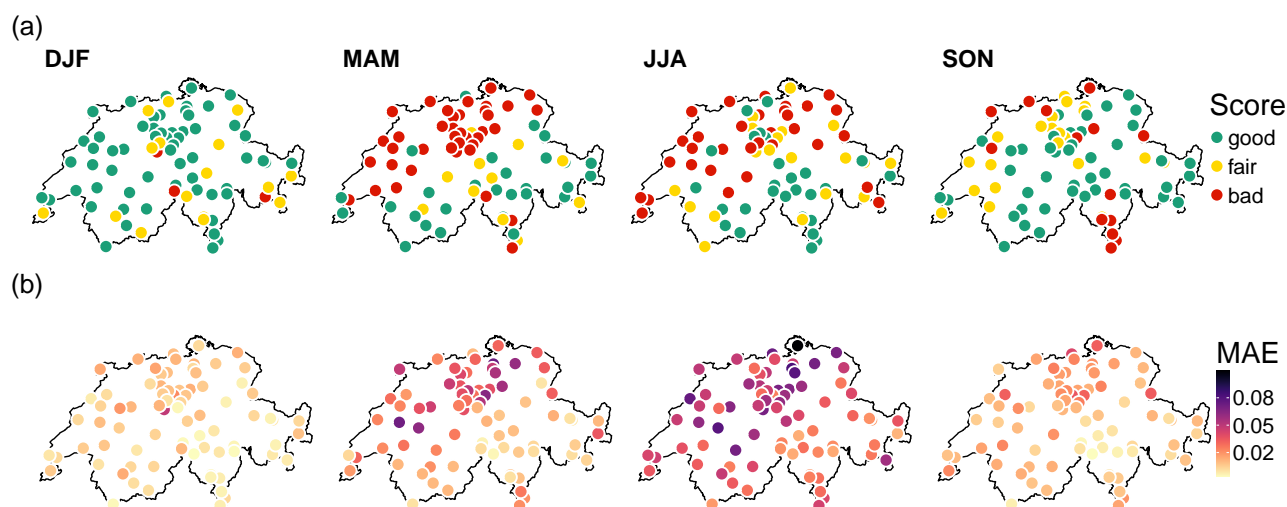
Figure 9. (a) Scores as assigned by CASE framework for the reproduction of 5-year return levels by model B for each site and each season. (b) Mean absolute errors (MAE) between observed and modelled p_x values for precipitation intensities higher than $1 \, \mathrm{mm \, h^{-1}}$ with model B, see equation (9).

6   Conclusions

470   According to many previous works, the distribution of the breakdown coefficients used in MRC models depends on a number of factors, including the temporal scale, precipitation intensity and the external pattern of the local precipitation sequence.

In the present study, we compare different MRC models, with/without the scaling dependency to the temporal scales, and with/without the scaling dependency to the external pattern of precipitation. Conversely to the scaling dependency to precipitation intensity and asymmetry, the scaling dependency to temporal scales reveals actually not obvious and its added value

475   in terms of model performance is much less clear than what was suggested in previous works. Moreover, accounting for a dependency on the temporal scales drastically increases the number of parameters to be estimated (+6 in the present case), which is especially expected to make the model much less robust and less appropriate for further regionalisation works.

The dependency on the external pattern of precipitation is shown to be important. In previous studies, it was accounted for with empirical models where the breakdown coefficient distribution was conditioned on different external pattern classes. To

480   our knowledge, although determinant, it was never accounted for in an analytical scaling framework, which also accounts for temporal scale and intensity dependencies. Our work presents a unified analytical MRC modelling framework that allows the cascade generator to depend in a continuous way on the temporal scale, precipitation intensity, and precipitation asymmetry.

Initially, we demonstrate the feasibility of characterizing the external precipitation pattern with a shadow breakdown coefficient, the so-called precipitation asymmetry index. We show that the larger the deviation of this index from 0.5 (index value

485   for a symmetrical precipitation configuration), the larger the asymmetry of the distribution of the breakdown coefficients. The relationships with this asymmetry index are modelled with two scaling sub-models. The first sub-model represents the dry probability asymmetry ratio φ that quantifies the asymmetry between p_{10} and p_{01}, i.e. the probabilities that all the precipitation amount is attributed exclusively either to the first or to the second subdivision, respectively. The second sub-model is related to the mean m of the positive breakdown coefficients distribution f_{W+}, which is equal to 0.5 is the asymmetry is disregarded.

490   These two sub-models lead to significant improvements for all statistics related to the temporal persistence and intermittency of precipitation, which are known to be difficult to simulate with standard MRC models. It has almost no influence on statistics related to precipitation distribution, such as standard deviations and precipitation extremes, e.g. return levels for given return periods.

Among the four different MRC models considered here, the one that accounts only for precipitation intensity and asymmetry

495   seems promising. It performs very well for all statistics considered, for all seasons and all temporal resolutions. It is, moreover, very parsimonious, with only five parameters. The five parameters are almost all independent from each other and can be estimated in a robust way, which avoids equifinality issues (Beven, 2006; Bárdossy, 2007). Whatever the parameter, the regional coherency is rather impressive. While all parameters present significant spatial variability reflecting the large variety of regional climates in Switzerland, the spatial variations of parameter estimates are very smooth. This suggests that a relevant regional

500   model will be possible for all parameters, allowing in turn the temporal disaggregation of coarse-resolution precipitation data anywhere in Switzerland. This disaggregation modelling framework is promising and could be also suited for other climate

contexts worldwide. Additional applications could help to better characterize its performance, its limitations, and its potential for regionalisation in such other contexts.

Code and data availability. The precipitation data used in this study are maintained by Swiss Federal Office of Meteorology and Climatology, MeteoSwiss (MeteoSwiss, 2021). It is available upon request at https://gate.meteoswiss.ch/idaweb/more.do (last accessed 10 December 2022).

The open-source code with routines allowing fitting and disaggregation of precipitation data based on the four MRC models presented in this study is available as an R package. It can be installed via GitHub: https://github.com/KaltrinaMaloku/disaggMRC.

Author contributions. Fund acquisition: BH; Data acquisition: KM; Experimental design: KM, BH, GE; Script development: KM, GE; model calibration, simulations and analyses: KM; Figures preparation: KM; Manuscript redaction: KM, BH, GE.

Competing interests. The authors declare no competing interests.

Acknowledgements. This research is part of the PhD thesis of Kaltrina Maloku. It has been supported by the Swiss Confederation, namely the Bundesamt fur Energie (grant no. SI/502150-01) and the Bundesamt fur Umwelt (grant no. SI/502150-01), through the project EXCH "Extreme floods in Switzerland".

Appendix A: Estimation of scaling model parameters

The parameters of the scaling models of each MRC model are estimated as follows:

- **Model A:** $p_x(I, \tau)$ is first estimated for different intensities classes I and temporal scales τ as the proportion of wet time steps where both subdivisions are wet (coloured dots in Figure 1a). These estimates are used to fit the relationships (7) for $\mu(\tau)$ and (8) for $\sigma(\tau)$ using the method of least square errors, which leads to estimates of the parameters a_μ, b_μ, a_σ and b_σ. For α, it is first estimated for different classes of intensity I and different temporal scales τ (coloured dots in Figure 1b) from the variance of the corresponding set of W^+'s by fitting a Beta distribution to the W^+ values with the method of moments (see equation (5)). It is also estimated for different classes of temporal scales τ (all intensities included; coloured dots in Figure 1c). The last estimates are used to fit the relationship (12) for $h(\tau)$ which lead to estimates of the parameters α_0 and H. In the third step, the ratio $\alpha(I, \tau)/h(\tau)$ is estimated for different classes of intensity and different temporal scales (coloured dots in Figure 1d). These estimates are used to fit the scaling model $g(I)$ of equation (13) which lead to estimates of the parameters c_0, c_1, c_2. An example of model fit for $p_x(I, \tau)$, for $g(I)$ and for $h(\tau)$, is given in Figure 1a, c and d respectively (plain lines).

- **Model B:** the estimation of model B follows a similar but more direct sequential process than for model A. In model B, p_x and α are assumed to only depend on the intensity I. In a first step, estimates of p_x (resp. α) are thus simply obtained for different classes of intensity (the empirical values of the W's calculated for all temporal scales are merged for the estimation). These p_x (resp α) estimates are then used to fit the scaling relationship (9) for $p_x(I)$ (resp. 13 for $\alpha(I)$) and obtain estimates of μ and σ (resp. K). An illustration is given in Figure 1b for α.

- **Model A$^+$/B$^+$:** Estimating the additional parameters related to the asymmetry follows an independent estimation process. Different φ and m estimates are first obtained for different z-index classes (all intensities and all time scales are merged for the estimation). For φ, these estimates are obtained from equation (15), while estimates of m are obtained as the mean of the W^+ values for different z-index classes. The scaling models (16) for $\varphi(z)$ and (17) for $m(z)$ are then fitted on these estimates, which leads to estimates of the parameters ν and λ, respectively. An example of fit is illustrated in Figure 3b-c. The different steps necessary to obtain p_{01}, and p_{01}, and the two parameters α_1, α_2 of the asymmetric Beta distribution are described in Sect. 2.4.

References

Acharya, S. C., Nathan, R., Wang, Q. J., and Su, C.-H.: Temporal disaggregation of daily rainfall measurements using regional reanalysis for hydrological applications, J. Hydrol., 610, 127 867, https://doi.org/10.1016/j.jhydrol.2022.127867, 2022.

Baeriswyl, P. A. and Rebetez, M.: Regionalization of precipitation in Switzerland by means of principal component analysis, Theor. Appl. Climatol., 58, 31–41, https://doi.org/10.1007/BF00867430, 1997.

Bennett, B., Thyer, M., Leonard, M., Lambert, M., and Bates, B.: A comprehensive and systematic evaluation framework for a parsimonious daily rainfall field model, J. Hydrol., 556, 1123–1138, https://doi.org/10.1016/j.jhydrol.2016.12.043, 2018.

Beven, K.: A manifesto for the equifinality thesis, J. Hydrol., 320, 18–36, https://doi.org/10.1016/j.jhydrol.2005.07.007, 2006.

Breinl, K. and Di Baldassarre, G.: Space-time disaggregation of precipitation and temperature across different climates and spatial scales, J. Hydrol. Reg. Stud., 21, 126–146, https://doi.org/10.1016/j.ejrh.2018.12.002, 2019.

Bárdossy, A.: Calibration of hydrological model parameters for ungauged catchments, Hydrol. Earth Syst. Sci., 11, 703–710, https://doi.org/10.5194/hess-11-703-2007, 2007.

Cristiano, E., ten Veldhuis, M.-C., and van de Giesen, N.: Spatial and temporal variability of rainfall and their effects on hydrological response in urban areas – a review, Hydrol. Earth Syst. Sci., 21, 3859–3878, https://doi.org/10.5194/hess-21-3859-2017, 2017.

Evin, G., Favre, A.-C., and Hingray, B.: Stochastic generation of multi-site daily precipitation focusing on extreme events, Hydrol. Earth Syst. Sci., 22, 655–672, https://doi.org/10.5194/hess-22-655-2018, 2018.

Frei, C. and Schär, C.: A precipitation climatology of the Alps from high-resolution rain-gauge observations, Int. J. Climatol., 18, 873–900, https://doi.org/10.1002/(SICI)1097-0088(19980630)18:8<873::AID-JOC255>3.0.CO;2-9, 1998.

Gringorten, I. I.: A plotting rule for extreme probability paper, J. Geophys. Res., 68, 813–814, https://doi.org/10.1029/JZ068i003p00813, 1963.

Güntner, A., Olsson, J., Calver, A., and Gannon, B.: Cascade-based disaggregation of continuous rainfall time series: the influence of climate, Hydrol. Earth Syst. Sci., 5, 145–164, https://doi.org/10.5194/hess-5-145-2001, 2001.

Hingray, B. and Ben Haha, M.: Statistical performances of various deterministic and stochastic models for rainfall series disaggregation, Atmos. Res., 77, 152–175, https://doi.org/10.1016/j.atmosres.2004.10.023, 2005.

Hingray, B., Picouet, C., and Musy, A., eds.: Hydrology: A Science for Engineers, CRC Press, 0 edn., https://doi.org/10.1201/b17169, 2014.

Hyndman, R. J. and Koehler, A. B.: Another look at measures of forecast accuracy, Int. J. Forecast., 22, 679–688, https://doi.org/10.1016/j.ijforecast.2006.03.001, 2006.

Jebari, S., Berndtsson, R., Olsson, J., and Bahri, A.: Soil erosion estimation based on rainfall disaggregation, J. Hydrol., 436-437, 102–110, https://doi.org/10.1016/j.jhydrol.2012.03.001, 2012.

Jennings, S. A., Lambert, M. F., and Kuczera, G.: Generating synthetic high resolution rainfall time series at sites with only daily rainfall using a master–target scaling approach, J. Hydrol., 393, 163–173, https://doi.org/10.1016/j.jhydrol.2010.08.013, 2010.

Kang, B. and Ramírez, J. A.: A coupled stochastic space-time intermittent random cascade model for rainfall downscaling, Water Resour. Res., 46, https://doi.org/10.1029/2008WR007692, 2010.

Koutsoyiannis, D. and Onof, C.: Rainfall disaggregation using adjusting procedures on a Poisson cluster model, J. Hydrol., 246, 109–122, https://doi.org/10.1016/S0022-1694(01)00363-8, 2001.

Liang, Q., Xia, X., and Hou, J.: Catchment-scale High-resolution Flash Flood Simulation Using the GPU-based Technology, Procedia Eng., 154, 975–981, https://doi.org/10.1016/j.proeng.2016.07.585, 2016.

McIntyre, N., Shi, M., and Onof, C.: Incorporating parameter dependencies into temporal downscaling of extreme rainfall using a random cascade approach, J. Hydrol., 542, 896–912, https://doi.org/10.1016/j.jhydrol.2016.09.057, 2016.

Menabde, M. and Sivapalan, M.: Modeling of rainfall time series and extremes using bounded random cascades and levy-stable distributions, Water Resour. Res., 36, 3293–3300, https://doi.org/10.1029/2000WR900197, 2000.

MeteoSwiss: Federal Office of Meteorology and Climatology, https://gate.meteoswiss.ch/idaweb/more.do, retrieved 12 December 2021, 2021.

Mezghani, A. and Hingray, B.: A combined downscaling-disaggregation weather generator for stochastic generation of multisite hourly weather variables over complex terrain: Development and multi-scale validation for the Upper Rhone River basin, J. Hydrol., 377, 245–260, https://doi.org/10.1016/j.jhydrol.2009.08.033, 2009.

Molnar, P. and Burlando, P.: Preservation of rainfall properties in stochastic disaggregation by a simple random cascade model, Atmos. Res., 77, 137–151, https://doi.org/10.1016/j.atmosres.2004.10.024, 2005.

Molnar, P. and Burlando, P.: Variability in the scale properties of high-resolution precipitation data in the Alpine climate of Switzerland: VARIABILITY IN SCALE PROPERTIES, Water Resour. Res., 44, https://doi.org/10.1029/2007WR006142, 2008.

Müller, H. and Haberlandt, U.: Temporal rainfall disaggregation using a multiplicative cascade model for spatial application in urban hydrology, J. Hydrol., 556, 847–864, https://doi.org/10.1016/j.jhydrol.2016.01.031, 2018.

Ochoa-Rodriguez, S., Wang, L.-P., Gires, A., Pina, R. D., Reinoso-Rondinel, R., Bruni, G., Ichiba, A., Gaitan, S., Cristiano, E., van Assel, J., Kroll, S., Murlà-Tuyls, D., Tisserand, B., Schertzer, D., Tchiguirinskaia, I., Onof, C., Willems, P., and ten Veldhuis, M.-C.: Impact of spatial and temporal resolution of rainfall inputs on urban hydrodynamic modelling outputs: A multi-catchment investigation, J. Hydrol., 531, 389–407, https://doi.org/10.1016/j.jhydrol.2015.05.035, 2015.

Olsson, J.: Evaluation of a scaling cascade model for temporal rain- fall disaggregation, Hydrol. Earth Syst. Sci., 2, 19–30, https://doi.org/10.5194/hess-2-19-1998, 1998.

Ormsbee, L. E.: Rainfall Disaggregation Model for Continuous Hydrologic Modeling, J. Hydraul. Eng., 115, 507–525, https://doi.org/10.1061/(ASCE)0733-9429(1989)115:4(507), 1989.

Park, H. and Chung, G.: A Nonparametric Stochastic Approach for Disaggregation of Daily to Hourly Rainfall Using 3-Day Rainfall Patterns, Water, 12, 2306, https://doi.org/10.3390/w12082306, 2020.

Paschalis, A., Molnar, P., and Burlando, P.: Temporal dependence structure in weights in a multiplicative cascade model for precipitation, Water Resour. Res., 48, https://doi.org/10.1029/2011WR010679, 2012.

Paschalis, A., Molnar, P., Fatichi, S., and Burlando, P.: On temporal stochastic modeling of precipitation, nesting models across scales, Advances in Water Resources, 63, 152–166, https://doi.org/10.1016/j.advwatres.2013.11.006, 2014.

Paulson, K. S. and Baxter, P. D.: Downscaling of rain gauge time series by multiplicative beta cascade, J. Geophys. Res., 112, D09 105, https://doi.org/10.1029/2006JD007333, 2007.

Pohle, I., Niebisch, M., Müller, H., Schümberg, S., Zha, T., Maurer, T., and Hinz, C.: Coupling Poisson rectangular pulse and multiplicative microcanonical random cascade models to generate sub-daily precipitation timeseries, J. Hydrol., 562, 50–70, https://doi.org/10.1016/j.jhydrol.2018.04.063, 2018.

Pui, A., Sharma, A., Mehrotra, R., Sivakumar, B., and Jeremiah, E.: A comparison of alternatives for daily to sub-daily rainfall disaggregation, J. Hydrol., 470-471, 138–157, https://doi.org/10.1016/j.jhydrol.2012.08.041, 2012.

R Core Team: R: A Language and Environment for Statistical Computing, R Foundation for Statistical Computing, Vienna, Austria, https://www.R-project.org/, 2022.

615 Rafieeinasab, A., Norouzi, A., Kim, S., Habibi, H., Nazari, B., Seo, D.-J., Lee, H., Cosgrove, B., and Cui, Z.: Toward high-resolution flash flood prediction in large urban areas – Analysis of sensitivity to spatiotemporal resolution of rainfall input and hydrologic modeling, J. Hydrol., 531, 370–388, https://doi.org/10.1016/j.jhydrol.2015.08.045, 2015.

Rupp, D. E., Keim, R. F., Ossiander, M., Brugnach, M., and Selker, J. S.: Time scale and intensity dependency in multiplicative cascades for temporal rainfall disaggregation, Water Resour. Res., 45, https://doi.org/10.1029/2008WR007321, 2009.

620 Rupp, D. E., Licznar, P., Adamowski, W., and Leśniewski, M.: Multiplicative cascade models for fine spatial downscaling of rainfall: parameterization with rain gauge data, Hydrol. Earth Syst. Sci., 16, 671–684, https://doi.org/10.5194/hess-16-671-2012, 2012.

Römkens, M. J. M., Helming, K., and Prasad, S. N.: Soil erosion under different rainfall intensities, surface roughness, and soil water regimes, CATENA, 46, 103–123, https://doi.org/10.1016/S0341-8162(01)00161-8, 2002.

Schertzer, D. and Lovejoy, S.: Physical modeling and analysis of rain and clouds by anisotropic scaling multiplicative processes, Journal of
625   Geophysical Research: Atmospheres, 92, 9693–9714, https://doi.org/10.1029/JD092iD08p09693, 1987.

Schleiss, M.: A new discrete multiplicative random cascade model for downscaling intermittent rainfall fields, Hydrol. Earth Syst. Sci., 24, 3699–3723, https://doi.org/10.5194/hess-24-3699-2020, 2020.

Seed, A. W., Srikanthan, R., and Menabde, M.: A space and time model for design storm rainfall, J. Geophys. Res., 104, 31 623–31 630, https://doi.org/10.1029/1999JD900767, 1999.

630 Segond, M.-L., Onof, C., and Wheater, H.: Spatial–temporal disaggregation of daily rainfall from a generalized linear model, J. Hydrol., 331, 674–689, https://doi.org/10.1016/j.jhydrol.2006.06.019, 2006.

Sikorska, A. E. and Seibert, J.: Appropriate temporal resolution of precipitation data for discharge modelling in pre-alpine catchments, Hydrol. Sci. J., 63, 1–16, https://doi.org/10.1080/02626667.2017.1410279, 2018.

Tessier, Y., Lovejoy, S., and Schertzer, D.: Universal Multifractals: Theory and Observations for Rain and Clouds, J. Appl. Meteorol. Climatol., 32, 223–250, https://doi.org/10.1175/1520-0450(1993)032<0223:UMTAOF>2.0.CO;2, 1993.
635

Viviroli, D., Sikorska-Senoner, A. E., Evin, G., Staudinger, M., Kauzlaric, M., Chardon, J., Favre, A.-C., Hingray, B., Nicolet, G., Raynaud, D., Seibert, J., Weingartner, R., and Whealton, C.: Comprehensive space–time hydrometeorological simulations for estimating very rare floods at multiple sites in a large river basin, Nat. Hazards Earth Syst. Sci., 22, 2891–2920, https://doi.org/10.5194/nhess-22-2891-2022, 2022.